Journal of Carbon Research

MDPI

Article

Carbon Nanotubes as Biosensors for Releasing Conjugated Bisphosphonates–Metal Ions in Bone Tissue: Targeted Drug Delivery through the DFT Method

Fatemeh Mollaamin [1,2,*] and Majid Monajjemi [3]

[1] Department of Food Engineering, Faculty of Engineering and Architecture, Kastamonu University, Kastamonu 37100, Turkey
[2] Department of Biology, Faculty of Science, Kastamonu University, Kastamonu 37100, Turkey
[3] Department of Chemical Engineering, Central Tehran Branch, Islamic Azad University, Tehran 1477893855, Iran
* Correspondence: smollaamin@gmail.com

Abstract: Bisphosphonate (BP) agents have attracted much attention for their precise therapy in some skeletal maladies demonstrated by enhancing osteoclast-mediated bone resorption. In this work, the use of CAM-B3LYP/6-311+G(d,p)/LANL2DZ to estimate the susceptibility of single-walled carbon nanotube (SWCNT) for adsorbing alendronate, ibandronate, neridronate, and pamidronate chelated to two metal cations of $2Mg^{2+}$, $2Ca^{2+}$, and $2Sr^{2+}$ through nuclear magnetic resonance and thermodynamic parameters has been accomplished. For most biological medications, oral bioavailability is too low to reach a therapeutic level, and advanced delivery systems such as formulations including permeation enhancers or enzyme inhibitors, lipid-based nanocarriers, and microneedles will likely increase the oral bioavailability of these medications properly. Therefore, the measurements have described that the eventuality of using SWCNT and BP agents becomes the norm in metal chelating of the drug delivery system, which has been selected through (alendronate, ibandronate, neridronate, pamidronate) $\rightarrow$ 2X (X = Mg^{2+}/Ca^{2+}/Sr^{2+}) complexes. The NMR results of chelated alendronate, ibandronate, neridronate, and pamidronate complexes adsorbed onto (5,5) armchair SWCNT have remarked the location of active sites of tagged nitrogen (N), phosphorus (S), oxygen (O), and metal cations of magnesium (Mg^{2+}), calcium (Ca^{2+}), and strontium (Sr^{2+}) in these molecules which replace the movement of the charge electron transfer in polar bisphosphonates (BPs) toward (5,5) armchair carbon nanotube (CNT). The thermodynamic results have exhibited that the substitution of $2Ca^{2+}$ cation by $2Sr^{2+}$ cation in the compound of the bioactive glasses can be efficient for treating vertebral complex fractures. However, the most fluctuation in the Gibbs free energy for BPs $\rightarrow$ $2Sr^{2+}$ has been observed at 300 K. This manuscript aimed to show that (5,5) armchair SWCNT can easily penetrate in the bone cells, delivering chelated BP–cations directly to the bone tissue. Drug delivery systems can improve the pharmacological profile, therapeutic profile, and efficacy of BP drugs and lower the occurrence of off-targets.

Keywords: drug delivery; bisphosphonate (BP); alendronate; ibandronate; neridronate; pamidronate; (5,5) armchair SWCNT; $2Mg^{2+}$; $2Ca^{2+}$; $2Sr^{2+}$

Citation: Mollaamin, F.; Monajjemi, M. Carbon Nanotubes as Biosensors for Releasing Conjugated Bisphosphonates–Metal Ions in Bone Tissue: Targeted Drug Delivery through the DFT Method. *C* **2023**, *9*, 61. https://doi.org/10.3390/c9020061

Academic Editors: Giuseppe Cirillo and Jandro L. Abot

Received: 27 February 2023
Revised: 16 May 2023
Accepted: 16 June 2023
Published: 19 June 2023

1. Introduction

The compounds of bisphosphonates (BPs) prevent the digestion of bones by pushing osteoclasts to bear cell death or apoptosis, which diminishes the velocity of bone destruction [1,2].

BP compounds stop bone resorption produced by different reasons in cells and organs. They prevent the formation of holes by isolating osteoclasts on mineral layers. The principal impact of active BPs is to prevent the resorption of bone tissue [3].

There is attention on enhancing the availability of biology and period of activity of a medication to modify remedial consequences. One of the applications of nanotechnology is in drug delivery, where nanoparticles are applied to carry and release drugs to a specific zone in the body. Targeted drug delivery is the delivery of a drug to its target site without having an effect on other tissues. Interest in targeted drug delivery has grown drastically due to its potential implications in the treatment of cancers and other chronic diseases. In order to achieve efficient targeted delivery, the designed system must avoid the host's defense mechanisms and circulate to its intended site of action. This drug delivery technique is able to change the pharmacology and particularity of a medication by adjusting it with various ingredients, medication carriers, and medical equipment [4].

BPs prevent the establishment, postpone the association, and decrease the solution of $Ca_3(PO_4)_2$ compounds. This notable characteristic is the foundation for the employment of these structures as a sign of the functionalized skeleton in nuclear medical sciences and the basis for their chosen localization in the bone tissue when employed as drugs [5–14]. The compounds of nanomedicine support a vast span of remedial demands, from nano drug delivery technology containing carbon nanostructures and the two-layered hydroxide to biological sensors in vitro and visualizing and implanting instruments in vivo through accurate diagnostics [15–23].

As shown by the exploration of CNTs in the 1990s and the progress of their applications in nanomedicine, these compounds possess significant properties, including rich electronic and thermal factors, great mechanical rigidity, high chemical resistance, and extremely light in weight [24–29].

The structures of nanotubes (NTs) with their natural attributes have been thought powerful applicants for drug delivery systems. The existence of capped ends of NTs might be opened up by oxidation, permitting the adhesion of molecules concerned with entry into the NT. Carbon nanotubes (CNTs) could lightly enter cells, releasing drugs straight into the nucleus or cytoplasm [30–46].

As a matter of fact, the most popular BP medications have a rich tension for metal cations, among them calcium cations, with which they can generate both soluble and insoluble compounds and aggregates relating to the pH of the solution and the existing metal [47–53].

Non-N-consisting BPs, such as clodronate, etidronate, and tiludronate, are discussed as the first generation of BPs, which are simple molecules including single atoms or alkyl groups in R1 and R2 side chains having a weak inhibition impact on bone resorption [54].

Adding an amino group introduced the start of the second generation of BPs that were more powerful, such as pamidronate as the first one, and other identical ones were pursued, where the situation of the nitrogen in the side chain was the clue to a more efficient medication [55].

Currently, the third generation of BPs, including N-containing heterocyclic BPs such as zoledronate and risedronate, have been presented. They have displayed the strongest antiresorptive attributes [56,57]. During the past years, the third generation of BPs with enhancing bone affinity has been brought up for osteoporosis and other bone disease treatments [58–60].

In this article, four second-generation BP agents containing alendronate, ibandronate, neridronate, and pamidronate, which have nitrogen (N) atoms in the side chain of R2 for promoting osteoclast apoptosis, have been investigated.

Alendronic acid ($C_4H_{13}NO_7P_2$) inhibits osteoclast-mediated bone resorption. Healthy bone tissue under therapy expands, and alendronate remains in the matrix of bone cells as an inactive pharmaco-figure. The best activity demands enough Ca element and vitamin D in the body to develop wholesome bone tissue [61–63].

Ibandronic acid ($C_9H_{23}NO_7P_2$) is also a second-generation BP medication, which is applied in the prohibition of and cures osteoporosis and deformation accompanied by skeletal fractures with cancer malady. It might likewise be employed to cure the increase in blood calcium levels in hypercalcemia [64,65].

Neridronic acid ($C_6H_{17}NO_7P_2$) is in a class of BP medications which is applied to cure imperfect osteogenesis and Paget's illness of bone cells [66,67].

Pamidronic acid ($C_3H_{11}NO_7P_2$) is another N-containing BP employed to prohibit osteoporosis and strengthen bones in Paget's disease. It is also employed to prevent bone loss, owing to steroid application, and in some cancers with high orientation to bone such as multiple myeloma. Due to its susceptibility to sequester Ca element in bone tissue, it is also applied to cure high amounts of Ca element and complex regional pain syndrome [68,69].

In this work, the chelation of BP agents of alendronate, ibandronate, neridronate, and pamidronate with $2Mg^{2+}$, $2Ca^{2+}$, and $2Sr^{2+}$ have been investigated in aqueous medium by forming relatively stable drugs for adsorption onto (5,5) armchair CNT as a drug delivery system (Scheme 1).

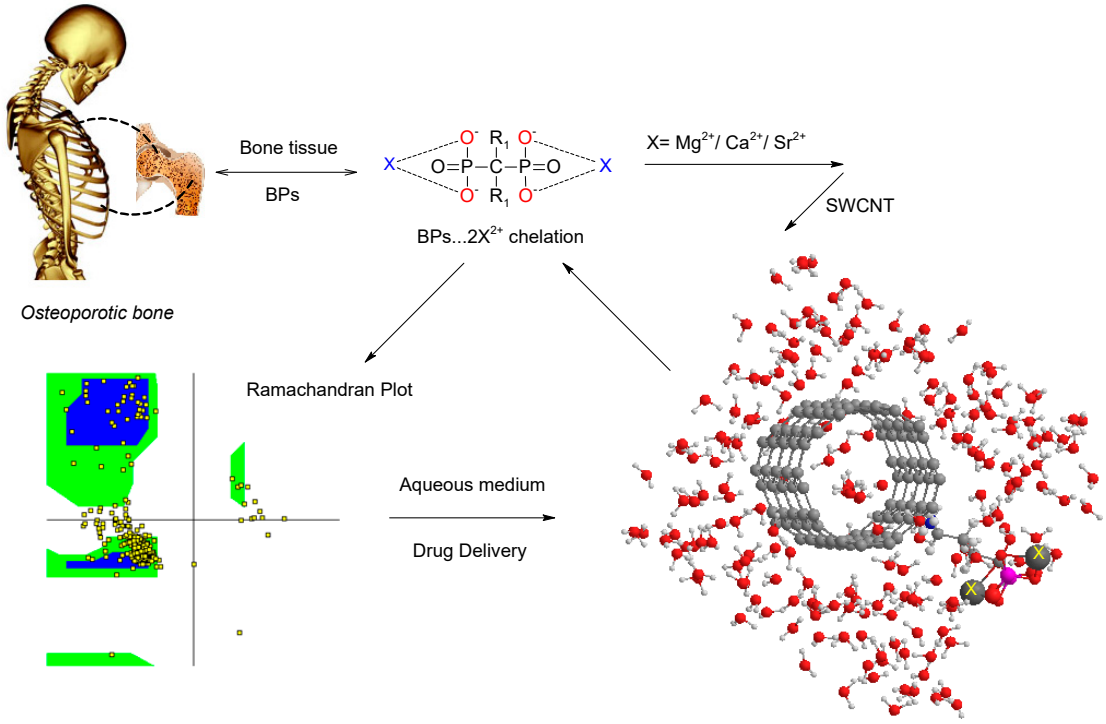

Scheme 1. Drug delivery of BP agents of alendronate, ibandronate, neridronate, and pamidronate chelated (**top-middle**) with regarding the Ramachandran Plot (**bottom-left**) to metal cations $2Mg^{2+}$, $2Ca^{2+}$, and $2Sr^{2+}$ (**top-right**) using (5,5) armchair SWCNT in aqueous medium (**bottom-right**) with for the treatment of osteoporotic bones (**top-left**) in the human body.

Then, a group of applied methods in quantum chemistry has been performed for detecting the optimum symmetry of [BP → $2Mg^{2+}$, $2Ca^{2+}$, $2Sr^{2+}$—(5,5) armchair CNT] chelation with the DFT method of computations using Gaussian 16 revision C.01 program package [70].

2. Design, Material, and Methods

In this investigation, the coordination geometries have been minimized at the insight of density functional theory by applying the three-parameter Becke's exchange [71] and Lee–Yang–Parr's correlation non-local functional [72], generally nominated as B3LYP method and basis sets of LANL2DZ by using Gaussian 16 revision C.01 program package [70] for two metal cations of Mg^{2+}, Ca^{2+}, and Sr^{2+} and 6-311+G(2d,p) for other atoms, including H, C, N, O, F, and P. Then, the electronic structure of adsorbed (5,5) armchair SWCNT by BP agents of alendronate, ibandronate, neridronate, and pamidronate chelated to $2Mg^{2+}$, $2Ca^{2+}$, and $2Sr^{2+}$ for measuring physico-chemical properties was described (Scheme 1).

DFT is one of the most employed approximations of Hohenberg, Kohn, and Sham, which permits the computational research of material attributes [73]. This theoretical method approves a beneficial system for estimating chemical mechanisms and understanding its resemblances and diversities to other computational applied approaches [74–77].

Moreover, the Onsager figure, progressed by Frisch, Wong and, Wiberg utilizing spherical cavities, has been accomplished. Although this method indicates a less detailed statement of the solute–solvent interface, this approximation simplifies the assessment of energy formatives in geometry coordination and frequency analysis. Furthermore, Cramer and Truhlar improved this pattern at the dipole surface [78–83].

Therefore, GIAO or the gauge including atomic orbitals has been accorded to work out the gauge problem in the computation of nuclear magnetic shielding for the complexes of alendronate, ibandronate, neridronate, and pamidronate chelated to $2Mg^{2+}$, $2Ca^{2+}$, and $2Sr^{2+}$ adsorbed onto (5,5) armchair SWCNT using DFT perspectives.

The chelation of BPs with cations in bone tissues was accomplished in this research by creating relatively stable complexes. Therefore, a group of quantum theoretical methods has been run to explore the minimized structures of [BP $\rightarrow$ $2Mg^{2+}$/$2Ca^{2+}$/$2Sr^{2+}$] cluster chelation adsorbed onto the surface of (5,5) armchair SWCNT as the drug delivery method in human bones, with thermodynamic calculations and nuclear magnetic resonance analysis using Gaussian 16 revision C.01 program [70,84–86].

3. Results

CNTs represent drug delivery platforms that can be functionalized with various biomolecules, including antibodies, proteins, and DNA. This permits the particular targeted transferring to special organs, cells, or tissues [87].

3.1. NMR Analysis

The computed results extracted from nuclear magnetic resonance (NMR) have indicated the SCF GIAO magnetic shielding tensor in ppm for oxygen, nitrogen, phosphorus, magnesium, calcium, and strontium exploring the active sites of alendronate, ibandronate, neridronate, and pamidronate complexes of BP agents as the medications for osteoporosis and analogous maladies cure. The calculations have been accomplished based on CAM-B3LYP/6-311+G (2d,p) order of theoretical computations due to Gaussian 16 revision C.01 software [70] and reported in Table 1.

The shielding parameters of NMR spectroscopy consisting of isotropic (σ_{iso}) and anisotropic tensors (σ_{aniso}) for alendronate, ibandronate, neridronate, and pamidronate chelated to metal cations of $2Mg^{2+}$, $2Ca^{2+}$, and $2Sr^{2+}$, which have been adsorbed onto (5,5) armchair SWCNT, have been estimated in Table 1.

In the aqueous medium, the agents of alendronate, ibandronate, neridronate, and pamidronate chelated to metal cations of $2Mg^{2+}$, $2Ca^{2+}$, and $2Sr^{2+}$ adsorbed onto (5,5) armchair SWCNT have approximately shown identical behavior for diverse atoms in the active zones of these complexes through the NMR qualities (Figure 1).

Alendronate, ibandronate, neridronate, and pamidronate chelated to $2Mg^{2+}$ have two sharp fluctuations in anisotropic shielding for oxygen atoms, while a steady state for other atoms, and especially for magnesium atoms (Figure 1a). Moreover, these BP agents chelated to $2Ca^{2+}$ have two sharp fluctuations in anisotropic shielding for oxygen atoms and a steady state for other atoms, while sharp peaks for calcium atoms have been observed (Figure 1b). Strontium atoms have shown sharp peaks through chelating to four mentioned BP units of osteoporosis drug (BP $\rightarrow$ $2Sr^{2+}$) using NMR anisotropic shielding (Figure 1c). The CS tensors are yielded by the quantum chemical calculations in fundamental axes system to estimate the isotropic chemical shielding (CSI), $(\sigma_{33} + \sigma_{22} + \sigma_{11})/3$, and anisotropic chemical shielding (CSA), $\sigma_{33} - (\sigma_{22} + \sigma_{11})/2$ [88].

Table 1. SCF GIAO magnetic shielding tensor for alendronate, ibandronate, neridronate, and pamidronate in ppm chelated to metal cations of $2Mg^{2+}$, $2Ca^{2+}$, and $2Sr^{2+}$ at the adsorption site onto (5,5) armchair SWCNT in aqueous medium.

Alendronate → $2Mg^{2+}$										
ppm	**P2**	**O3**	**P4**	**O5**	**O6**	**O7**	**O8**	**N14**	**Mg15**	**Mg16**
σ_{iso}	476.9364	354.2408	526.9666	201.1994	417.9254	272.9464	338.2907	295.2486	476.8934	449.8215
σ_{aniso}	197.3153	94.4458	209.7908	927.3699	1271.225	109.1100	1160.4760	32.8868	273.6673	317.7684
Alendronate → $2Ca^{2+}$										
ppm	**P2**	**O3**	**P4**	**O5**	**O6**	**O7**	**O8**	**N14**	**Ca15**	**Ca16**
σ_{iso}	560.1002	352.9742	533.0987	133.3365	238.4170	122.0996	273.4535	299.2374	1266.8935	1242.6875
σ_{aniso}	144.2001	63.4751	247.7018	359.3426	291.6360	636.0180	369.2229	32.2780	190.3530	186.0608
Alendronate → $2Sr^{2+}$										
ppm	**P2**	**O3**	**P4**	**O5**	**O6**	**O7**	**O8**	**N14**	**Sr15**	**Sr16**
σ_{iso}	578.0939	398.6744	560.6582	378.7838	392.6713	389.2691	392.7619	299.5870	3153.5958	3230.1562
σ_{aniso}	184.7045	69.5146	177.8449	205.3841	221.1451	243.9178	248.8879	28.5730	257.5701	204.4964
Ibandronate → $2Mg^{2+}$										
ppm	**O1**	**P3**	**O4**	**O5**	**O6**	**P7**	**O8**	**N13**	**Mg19**	**Mg20**
σ_{iso}	362.9223	418.1065	59.9740	34.3478	138.1868	424.7443	36.0918	293.6687	537.7617	523.1200
σ_{aniso}	57.8641	147.7471	487.9605	510.3891	728.4770	174.0288	439.9294	38.7725	159.6272	203.9691
Ibandronate → $2Ca^{2+}$										
ppm	**O1**	**P3**	**O4**	**O5**	**O6**	**P7**	**O8**	**N13**	**Ca19**	**Ca20**
σ_{iso}	361.5829	210.1687	452.6134	669.4192	677.6753	349.5293	187.1626	293.1990	1221.7390	1150.9306
σ_{aniso}	57.0125	394.7186	1378.5036	1425.4072	1457.4494	227.4777	899.2902	40.5514	199.6107	372.1082
Ibandronate → $2Sr^{2+}$										
ppm	**O1**	**P3**	**O4**	**O5**	**O6**	**P7**	**O8**	**N13**	**Sr19**	**Sr20**
σ_{iso}	365.6022	331.3843	317.9684	408.4177	228.0619	426.3955	120.2419	292.7850	3130.9451	3039.3312
σ_{aniso}	69.4799	209.7331	1123.9718	1191.6414	831.6244	98.9009	819.3784	40.7449	250.0123	505.0866
Neridronate → $2Mg^{2+}$										
ppm	**O1**	**P3**	**O4**	**O5**	**O6**	**P7**	**O8**	**N16**	**Mg17**	**Mg18**
σ_{iso}	362.0412	411.7829	40.1498	88.5579	183.8948	435.2663	43.0977	298.1960	528.3357	534.3457
σ_{aniso}	57.1142	162.3461	533.2377	448.0810	788.6783	107.3363	452.0056	29.1476	183.6469	184.4351
Neridronate → $2Ca^{2+}$										
ppm	**O1**	**P3**	**O4**	**O5**	**O6**	**P7**	**O8**	**N16**	**Ca17**	**Ca18**
σ_{iso}	361.1504	295.8674	284.3469	313.0876	419.9667	375.6348	181.9129	297.5033	1183.2441	1202.8418
σ_{aniso}	55.2182	263.4852	1198.8384	1051.2597	1099.8941	177.8481	875.2833	29.3969	288.6887	231.3930
Neridronate → $2Sr^{2+}$										
ppm	**O1**	**P3**	**O4**	**O5**	**O6**	**P7**	**O8**	**N16**	**Sr17**	**Sr18**
σ_{iso}	367.1523	390.6068	40.0323	9.2850	152.4282	390.9190	32.2100	298.4373	3061.4067	3101.5619
σ_{aniso}	73.7996	126.9946	858.7106	697.0640	720.7286	138.6716	689.5901	30.3294	246.8092	175.3476
Pamidronate → $2Mg^{2+}$										
ppm	**O1**	**P3**	**O4**	**O5**	**O6**	**P7**	**O8**	**N13**	**Mg14**	**Mg15**
σ_{iso}	362.0592	381.0455	66.9541	29.6460	279.2352	403.3851	8.7584	298.0285	522.9221	515.9499
σ_{aniso}	61.9317	198.8411	474.8645	486.8028	909.1096	153.6341	465.7539	29.4898	201.9489	227.1125
Pamidronate → $2Ca^{2+}$										
ppm	**O1**	**P3**	**O4**	**O5**	**O6**	**P7**	**O8**	**N13**	**Ca14**	**Ca15**
σ_{iso}	363.4157	308.7031	139.8592	313.4116	335.8527	302.3324	368.3457	298.7044	1180.3416	1195.3529
σ_{aniso}	55.7660	229.5383	992.3576	852.3174	963.5384	253.4179	812.8236	30.5223	259.1125	268.9893
Pamidronate → $2Sr^{2+}$										
ppm	**O1**	**P3**	**O4**	**O5**	**O6**	**P7**	**O8**	**N13**	**Sr14**	**Sr15**
σ_{iso}	363.8761	241.3363	515.8675	557.2093	446.4313	382.1276	109.8785	296.7719	3017.4505	3053.8428
σ_{aniso}	65.8230	339.8384	1283.1154	1420.8103	1145.4648	144.3417	846.5852	31.5079	558.2663	370.8348

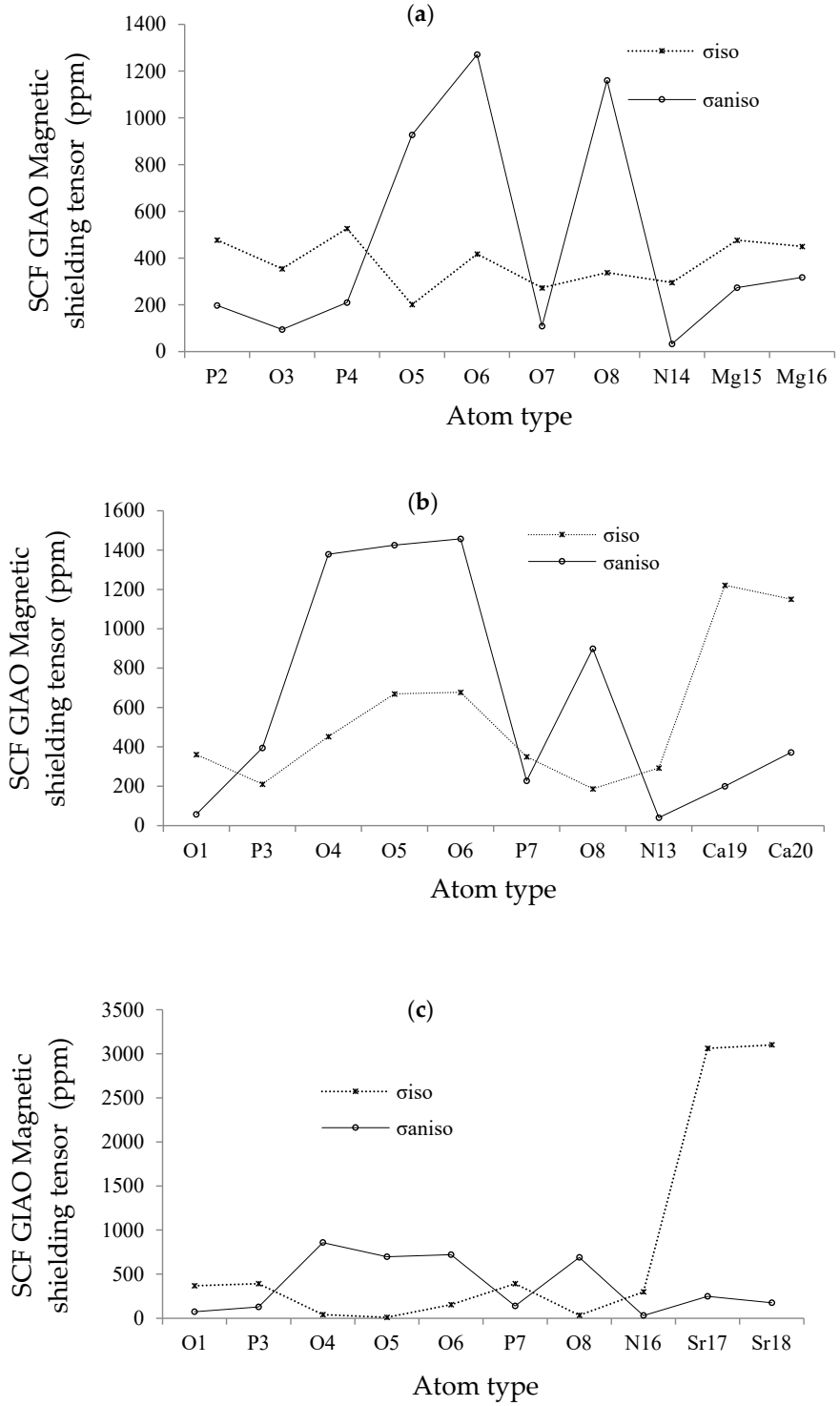

Figure 1. ^{13}C-NMR shielding of isotropic (σ_{iso}) and anisotropic (σ_{aniso}) tensors calculated for (**a**) BPs-Mg^{2+}, (**b**) BPs-Ca^{2+}, and (**c**) BPs-Sr^{2+} using the SCF GIAO method due to CAM-B3LYP function and LANL2DZ basis set for metal cations and 6-311+G(2d,p) basis set for further atoms through electronegative atoms of N, O, and P as the active positions in the structures of BP agents.

In addition, the Onsager model has influenced NMR traits and shielding tensors of H, C, N, O, P, Mg, Ca, and Sr atoms in chelated alendronate, ibandronate, neridronate, and pamidronate (Figure 2). In the results of ^{1}H-NMR spectroscopy in Figure 2, the fluctuation of chemical shielding using nuclear magnetic resonance for these chelated BPs is shown.

As a matter of fact, alendronate, ibandronate, and neridronate have shown NMR shielding between 10–1400 ppm with a sharp peak in 25 ppm and several weak peaks between 200–400 ppm (Figure 2a–c). Pamidronate has NMR shielding between 10–600 ppm with a sharp peak in 25 ppm and several weak peaks between 200–400 ppm (Figure 2d).

In addition, in Figure 2a–d, an electrostatic potential (ESP) surface or map of a molecule that presents the partial distribution of change along the molecule's surface, which helps to assign molecular polarity, has been shown.

The outlook of Figure 2 suggests the proof for standing a variety of measurements for chelated alendronate, ibandronate, neridronate, and pamidronate complexes adsorbed onto (5,5) armchair SWCNT, which presents the location of active zones of targeted atoms of N, P, O, and metal cations of Mg^{2+}, Ca^{2+}, and Sr^{2+} in these molecules that replace the charge transfer factor in polar BPs toward (5,5) armchair CNT.

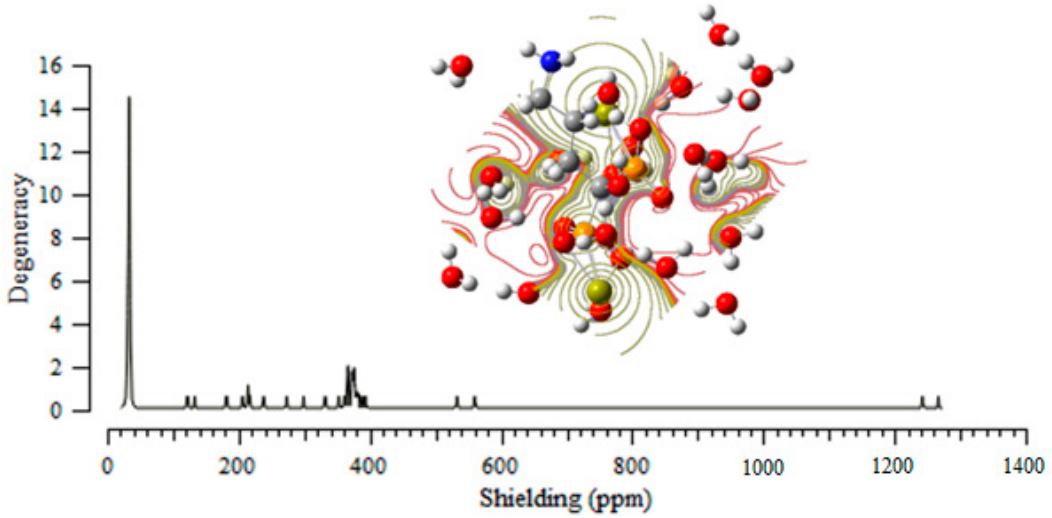

(**a**)

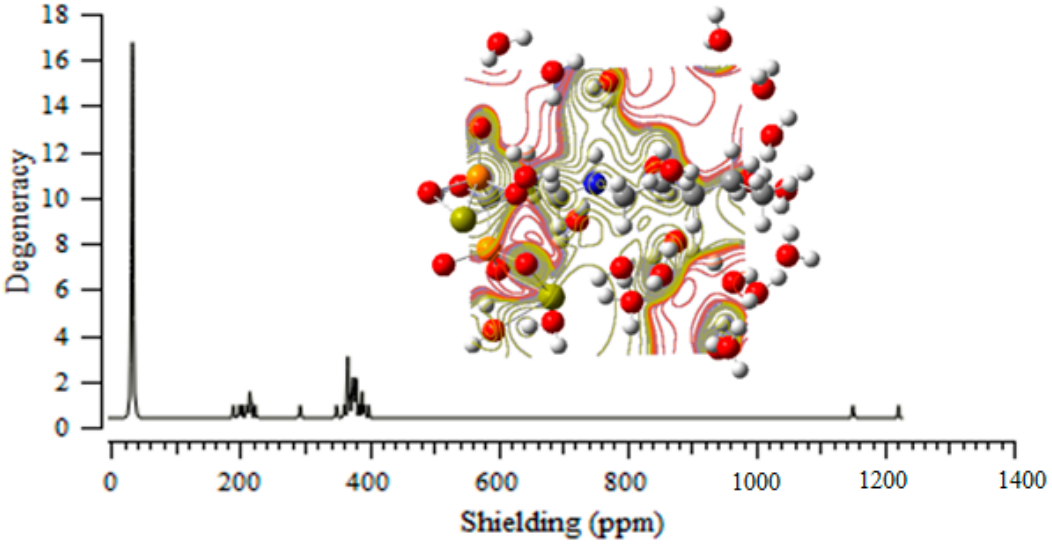

(**b**)

Figure 2. *Cont.*

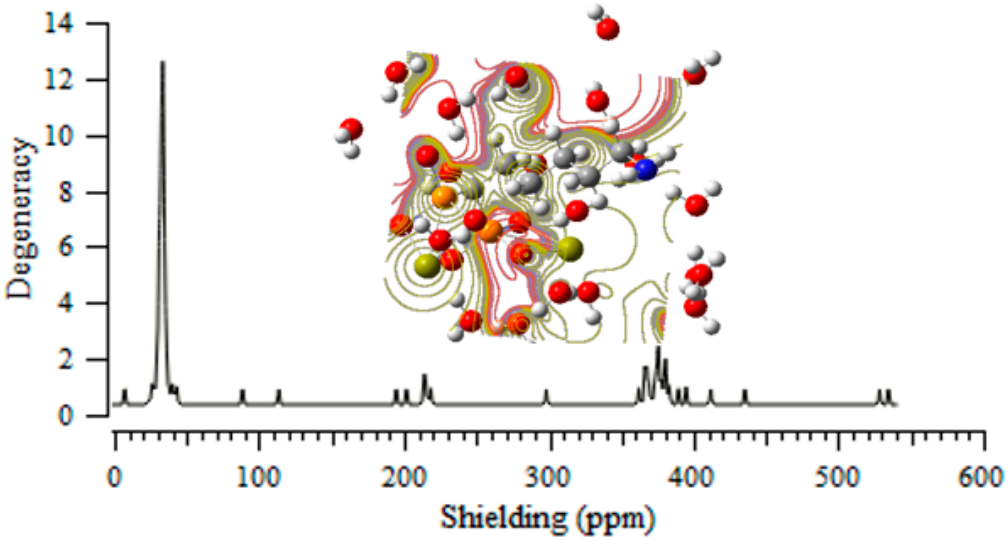

(**c**)

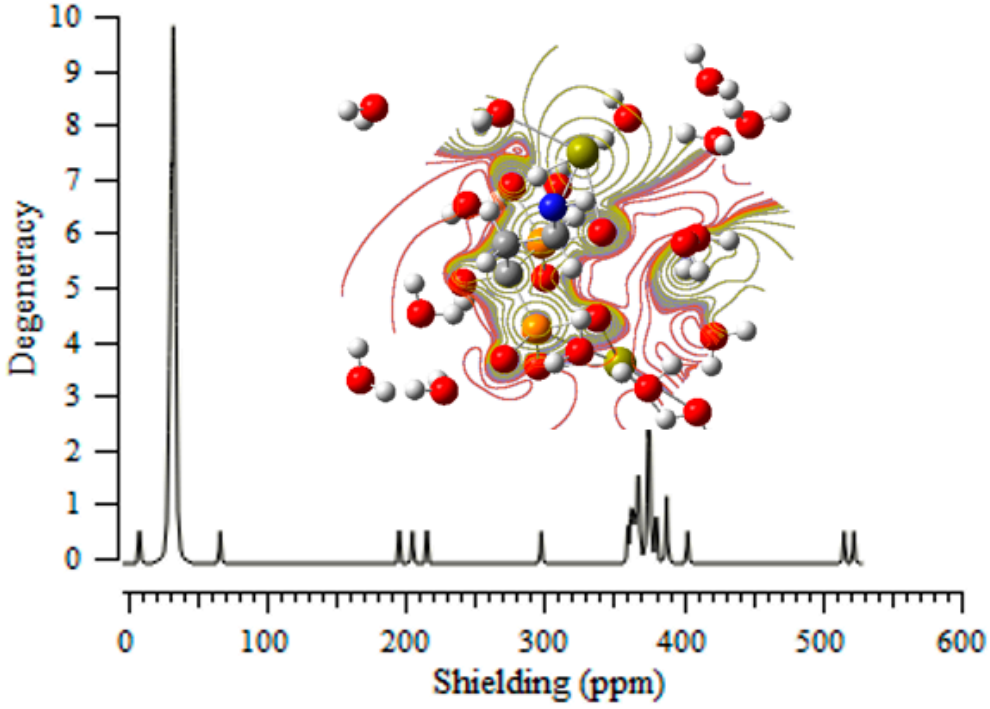

(**d**)

Figure 2. ^{1}H-NMR shielding and ESP map of (**a**) alendronate-X^{2+}, (**b**) ibandronate-X^{2+}, (**c**) neridronate-X^{2+}, and (**d**) pamidronate-X^{2+} using the SCF GIAO method due to B3LYP function and lnl2dz basis set for metal cations (X^{2+}), including Mg^{2+}, Ca^{2+}, and Sr^{2+},and 6-311+G(2d,p) basis set basis set for alternative atoms.

3.2. Nuclear Quadrupole Resonance (NQR)

In NMR, nuclei with spin $\geq 1/2$ have a magnetic dipole moment so that their energies are split by a magnetic field, permitting resonance sorption of energy dependent on the Larmor frequency; $\omega_L = \gamma B$, where γ is the gyromagnetic ratio and B is the magnetic field external to the nucleus.

As the electric field gradient (EFG) at the position of the nucleus in organic inhibitors is assigned by the valence electrons twisted in the special linkage with close nuclei of aluminum surface, the NQR frequency at which transitions happen is particular for BPs

(alendronate/ibandronate/neridronate/pamidronate) → 2X (X = Mg^{2+}/$2Ca^{2+}$/$2Sr^{2+}$) complexes in aqueous medium (Table 2).

Table 2. The electric potential for elements of BPs → 2Mg2+/2Ca2+/2Sr2+ in aqueous medium that have been adsorbed on the SWCNT surface by CAM-B3LYP/EPR-III,6-31+G(d,p), LANL2DZ calculations extracted from the NQR method.

Atom Type	Alendronate-$2Mg^{2+}$	Alendronate-$2Ca^{2+}$	Alendronate-$2Sr^{2+}$	Atom Type	Pamidronate-$2Mg^{2+}$	Pamidronate-$2Ca^{2+}$	Pamidronate-$2Sr^{2+}$
C1	−14.582015	−14.680364	−14.698286	O1	−22.089153	−22.112109	−22.145726
P2	−53.374813	−53.279858	−53.29495	C2	−14.579306	−14.602032	−14.638223
O3	−22.058521	−22.149621	−22.098919	P3	−53.406411	−53.417423	−53.477559
P4	−53.376494	−53.282896	−53.27529	O4	−22.272632	−22.279084	−22.336336
O5	−22.244579	−22.278534	−22.394044	O5	−22.258221	−22.248791	−22.343459
O6	−22.229734	−22.286302	−22.390886	O6	−22.456859	−22.462141	−22.517174
O7	−22.431022	−22.429008	−22.442474	P7	−53.376249	−53.408809	−53.453886
O8	−22.239543	−22.278605	−22.412946	O8	−22.233854	−22.239144	−22.352915
O9	−22.204363	−22.27527	−22.397572	O9	−22.229882	−22.285782	−22.304591
O10	−22.40249	−22.456515	−22.473484	O10	−22.408516	−22.432219	−22.484225
C11	−14.561176	−14.600068	−14.578144	C11	−14.564672	−14.577927	−14.601869
C12	−14.543709	−14.561792	−14.530637	C12	−14.545795	−14.572535	−14.576751
C13	−14.51357	−14.520012	−14.514399	N13	−18.152349	−18.171899	−18.160602
N14	−18.130473	−18.146224	−18.128618	X14	−39.095005	−79.482876	−194.832492
X15	−39.09341	−79.466582	−194.914058	X15	−39.061118	−79.461646	−194.815758
X16	−39.093721	−79.477353	−194.90834				
Atom Type	**Ibandronate-$2Mg^{2+}$**	**Ibandronate-$2Ca^{2+}$**	**Ibandronate-$2Sr^{2+}$**	**Atom Type**	**Neridronate-$2Mg^{2+}$**	**Neridronate-$2Ca^{2+}$**	**Neridronate-$2Sr^{2+}$**
O1	−22.071174	−22.090505	−22.135028	O1	−22.063309	−22.079958	−22.162592
C2	−14.55445	−14.576253	−14.627075	C2	−14.546229	−14.565095	−14.661299
P3	−53.377051	−53.398859	−53.464651	P3	−53.378029	−53.393132	−53.507653
O4	−22.232796	−22.250951	−22.326769	O4	−22.239304	−22.250603	−22.39611
O5	−22.232416	−22.226345	−22.32228	O5	−22.234969	−22.224863	−22.37294
O6	−22.410299	−22.442602	−22.498632	O6	−22.417286	−22.426463	−22.551375
P7	−53.353291	−53.373911	−53.437238	P7	−53.324873	−53.342394	−53.469496
O8	−22.219745	−22.241599	−22.327087	O8	−22.191646	−22.214617	−22.352985
O9	−22.212105	−22.212723	−22.310918	O9	−22.19086	−22.188493	−22.348579
O10	−22.383435	−22.380158	−22.417829	O10	−22.316029	−22.340715	−22.505319
C11	−14.548019	−14.564822	−14.601757	C11	−14.539276	−14.556356	−14.627277
C12	−14.53678	−14.558542	−14.589055	C12	−14.558729	−14.581511	−14.640502
N13	−18.142608	−18.152869	−18.17498	C13	−14.539792	−14.555941	−14.587432
C14	−14.514959	−14.514147	−14.525321	C14	−14.530353	−14.543764	−14.562173
C15	−14.553135	−14.541599	−14.550868	C15	−14.505909	−14.512938	−14.524351
C16	−14.547176	−14.534201	−14.545824	N16	−18.138051	−18.139505	−18.150542
C17	−14.54458	−14.532666	−14.552941	X17	−39.064255	−79.461993	−194.854003
C18	−14.542677	−14.536273	−14.550469	X18	−39.016632	−79.412003	−194.820676
X19	−39.028844	−79.428857	−194.800917				
X20	−39.063707	−79.469808	−194.822286				

Moreover, the electric potential through transferring of electric charge from one site to another site in the presence of an electric field has been measured for BPs (alendronate/ibandronate/neridronate/pamidronate) → 2X (X = Mg^{2+}/Ca^{2+}/Sr^{2+}) complexes using CAM-B3LYP/EPR-III, 6-31+G(d,p), LANL2DZ level of theory (Figure 3). Therefore, in Figure 3, the electric potential of the NQR method for elements of C, O, N, P, Mg, Ca, and Sr dealing with interaction sites between BPs and chelated metallic cations in aqueous medium has been plotted.

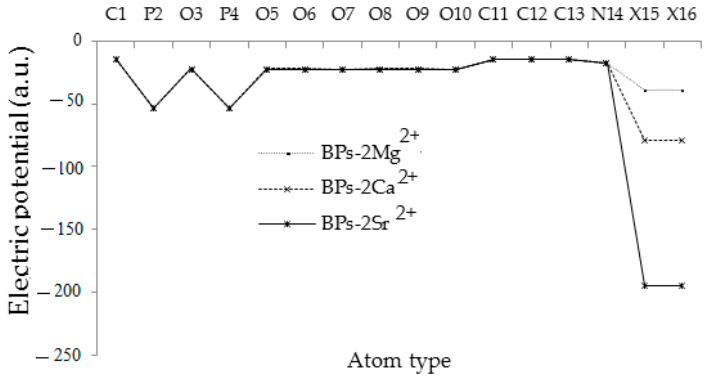

Figure 3. The changes of the electric potential versus atomic charge through NQR calculations for BPs (alendronate/ibandronate/neridronate/pamidronate) → $2Mg^{2+}/2Ca^{2+}/2Sr^{2+}$ in aqueous medium adsorbed on the SWCNT surface by CAM-B3LYP/EPR-III,6-31+G(d,p), LANLD2Z calculations extracted from the NQR method (Note: X = Mg/Ca/Sr).

There is an electric quadrupole moment in NQR, nuclei with spin ≥ 1, which is accompanied by non-spherical nuclear charge distributions. So, the nuclear charge repartition digresses from that of a sphere as the oblate or prolate form of the nucleus [89,90].

Therefore, the NQR transition frequencies are symmetric to the electric quadrupole moment of the nucleus and the scale of the strength of the local EFG: $\omega \sim \frac{e^2 Qq}{\hbar} = C_q$, where q is dependent on the biggest fundamental portion of the EFG tensor at the nucleus, and C_q is the quadrupole coupling constant parameter [89,90].

The NQR method is based on the multipole expansion in Cartesian coordinates as the following equations:

$$V(r) = V(0) + \left[\left(\frac{\partial V}{\partial x_i}\right)\Big|_0 \cdot x_i\right] + \frac{1}{2}\left[\left(\frac{\partial^2 V}{\partial x_i x_j}\right)\Big|_0 \cdot x_i x_j\right] + \cdots \quad (1)$$

Then, after simplification of the equation, there are only the second derivatives dependent on the same variable for the potential energy [89–92]:

$$\begin{aligned} U = -\tfrac{1}{2} \int_{\mathcal{D}} d^3 r\, \rho_r \left[\left(\frac{\partial^2 V}{\partial x_i^2}\right)\Big|_0 \cdot x_i^2\right] = -\tfrac{1}{2} \int_{\mathcal{D}} d^3 r\, \rho_r \left[\left(\frac{\partial E_i}{\partial x_i}\right)\Big|_0 \cdot x_i^2\right] \\ = -\tfrac{1}{2} \left(\frac{\partial E_i}{\partial x_i}\right)\Big|_0 \cdot \int_{\mathcal{D}} d^3 r\, [\rho(r) \cdot x_i^2] \end{aligned} \quad (2)$$

The effect of the substitution of metal cations of $2Mg^{2+}/2Ca^{2+}/2Sr^{2+}$ chelated to BPs adsorbed onto (5,5) armchair SWCNT through resulted electric potential using NQR analysis (Table 2 and Figure 3) has been observed. It is obvious that the graph of NQR characteristics for BPs (alendronate/ibandronate/neridronate/pamidronate) → $2Mg^{2+}/2Ca^{2+}/2Sr^{2+}$ has the most fluctuation in the region of magnesium, calcium, and strontium (Figure 3).

3.3. Physical and Thermochemical Properties

The physical and chemical properties of dipole moment (Debye), Virial coefficient (-V/T), relative energy (kcal/mol), and Gibbs free energy (kcal/mol) have determined the stability of BP agents among the chelated BPs, including alendronate/ibandronate/neridronate/pamidronate → $2Mg^{2+}/2Ca^{2+}/2Sr^{2+}$ adsorbed onto (5,5) armchair SWCNT as the medications for excluding the damage of bone tissues and curing osteoporosis and other relevant maladies through the chelated bonding of these complexes with Mg^{2+}, Ca^{2+}, and Sr^{2+} using the drug delivery procedure (Table 3).

Table 3. Physico-chemical characteristics of chelated agents of BPs with each of two metal cations of Mg^{2+}, Ca^{2+}, and Sr^{2+}, respectively, adsorbed onto (5,5) armchair SWCNT in aqueous medium at 300 K.

BPs Agent	Metal Cation	Relative Energy $\times 10^{-4}$ (kcal/mol)	Gibbs Free Energy $\times 10^{-4}$ (kcal/mol)	Virial Coefficient (-V/T)	Dipole Moment (Debye)
Alendronate	$2Mg^{2+}$	−105.3238	−208.3444	1.9576	5.0901
	$2Ca^{2+}$	−157.7413	−278.2509	1.9129	3.2620
	$2Sr^{2+}$	−471.0163	−632.8529	1.9999	5.2236
Ibandronate	$2Mg^{2+}$	−101.7982	−240.3687	1.8233	19.5703
	$2Ca^{2+}$	−159.7855	−315.8492	1.8691	22.2388
	$2Sr^{2+}$	−482.5812	−683.2521	2.0030	28.8543
Neridronate	$2Mg^{2+}$	−102.8331	−226.2752	1.8789	18.4846
	$2Ca^{2+}$	−161.3368	−301.3348	1.9021	20.1825
	$2Sr^{2+}$	−471.6486	−654.1330	1.9908	28.9546
Pamidronate	$2Mg^{2+}$	−95.8092	−195.2457	1.8754	16.0488
	$2Ca^{2+}$	−164.3777	−278.4610	1.9726	18.5122
	$2Sr^{2+}$	−472.0945	−624.2867	2.0052	34.5252

Figure 4 has exhibited that the fluctuation of relative energy in front of the Virial coefficient (-V/T) for BPs of alendronate/ibandronate/neridronate/pamidronate chelated to $2Mg^{2+}$, $2Ca^{2+}$, $2Sr^{2+}$ adsorbing onto (5,5) armchair SWCNT in aqueous medium, which was optimized by ab initio approach accompanying CAM-DFT functional consisting of ECP computations with theoretical status of LANL2DZ for metal elements.

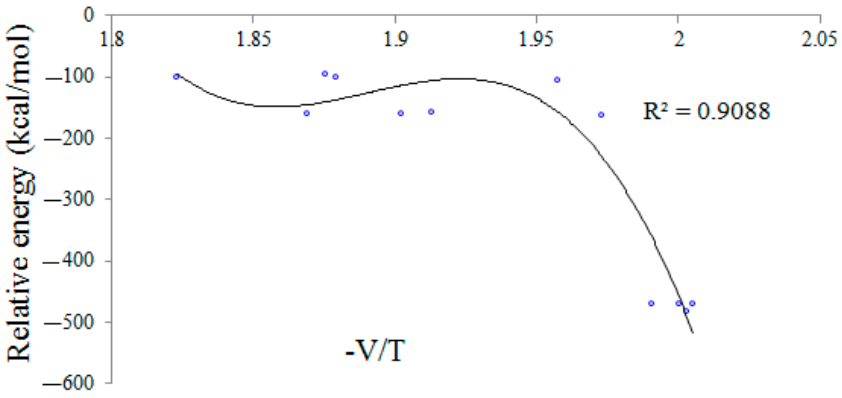

Figure 4. Changes of relative energy versus Virial coefficient (-V/T) for chelated BP agents with two metal cations of Mg^{2+}, Ca^{2+}, and Sr^{2+} adsorbed onto (5,5) armchair SWCNT in aqueous medium at 300 K.

In Figure 4, it has been observed that with increasing Virial coefficient, the relative energy for (alendronate/ibandronate/neridronate/pamidronate) → $2Mg^{2+}$/$2Ca^{2+}$/$2Sr^{2+}$ adsorbed onto (5,5) armchair SWCNT is reduced, with a relation coefficient of R^2 = 0.9088.

The observed consequences strongly propose that the various measurements derived from BP agents in the solvent are mainly because basis sets are persuaded by an alteration in the polarity of the ambience. It is obvious that an enhancement in the dielectric constants augments the resistance and efficiency of these BP medications for prohibiting the damage of bone density and remedying osteoporosis (Figure 5).

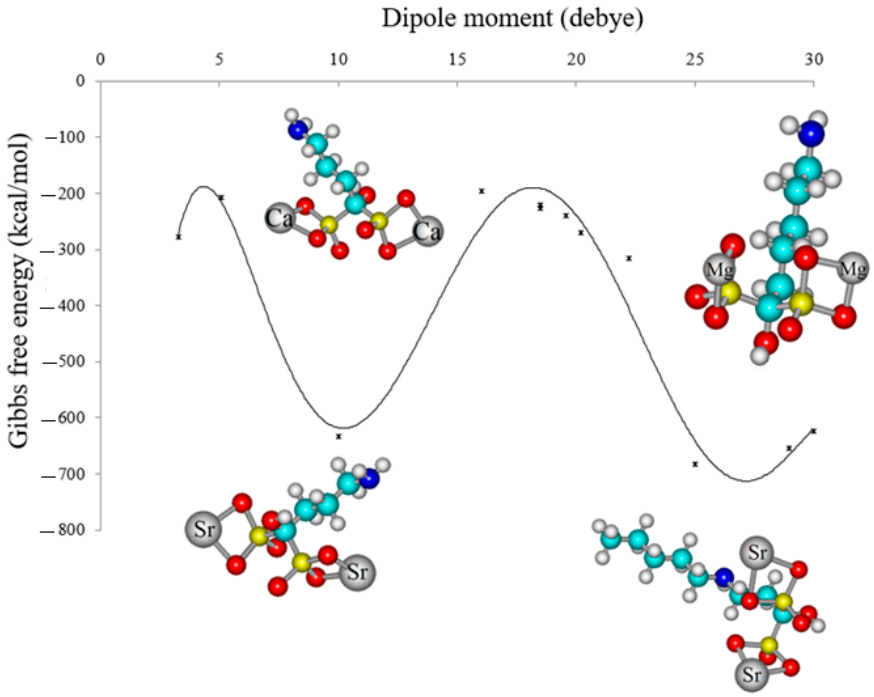

Figure 5. The changes of Gibbs free energy (ΔG_R^o) (kcal/mol) versus dipole moment (Debye) for chelated BP agents with two metal cations of Mg^{2+}, Ca^{2+}, and Sr^{2+} adsorbed onto (5,5) armchair SWCNT in aqueous medium at 300 K.

Strontium (Sr) is famous for its capability to increase bone and teeth mineralization, osteogenesis, and angiogenesis and downgrade osteoclast activity. This element, as one of the principal compounds of bone tissue, has a straight impact on the metabolism of the bone. For improving bone treatments, various investigations have concentrated on the exchange of Ca^{2+} cations by strontium ions in the compound of bioactive glasses, which can be used to cure vertebral complex fractures [93,94]. In Figure 5, BPs chelated to strontium (Sr) have shown the most fluctuation in Gibbs free energy with dipole moments in the aqueous medium at 300 K.

From Figure 5, the minimum values based on ΔG_R^o versus dipole moment might relate to the interactions between the chelated BP structures in the aqueous medium and the CNT surface. In fact, by comparing to ΔG_R^o amounts, an acceptable accord among computed consequences has been approved, as well as the accuracy of the chosen isotherm for (alendronate/ibandronate/neridronate/pamidronate) $\rightarrow 2Mg^{2+}/2Ca^{2+}/2Sr^{2+}$ adsorbed onto (5,5) armchair SWCNT in aqueous medium, which is approved by the following equation:

$$\Delta G_R^o = \Delta G^o_{BPs-2X^{2+}\rightarrow CNT} - \left(\Delta G^o_{BPs} + \Delta G^o_{2X^{2+}} + \Delta G^o_{CNT}\right); X = Mg, Ca, Sr \quad (3)$$

On the basis of data in Table 3, it is predicted that the adsorption of BPs-$2X^{2+}$ (X = Mg, Ca, Sr) on the CNT may be physical or chemical in nature. As seen in Table 3, all the evaluated ΔG_R^o amounts are mostly close, exhibiting the settlement of the figured parameters by all approaches and the reliability of the measurements.

3.4. LUMO and HOMO (Frontier Orbital)

The frontier orbitals of LUMO and HOMO as the lowest unoccupied molecular orbital and highest occupied molecular orbital, respectively, have been calculated for BP agents of alendronate, ibandronate, neridronate, and pamidronate chelated to $2Mg^{2+}$, $2Ca^{2+}$, and $2Sr^{2+}$ adsorbing onto (5,5) armchair SWCNT in aqueous medium accompanying CAM-B3LYP/6-31+G (2d,p), EPR-III, LANL2DZ (Table 4).

Table 4. The LUMO (a.u.), HOMO (a.u.), band energy gap (ΔE/ev), and other qualifications (ev) for (alendronate/ibandronate/neridronate/pamidronate) → $2Mg^{2+}$/$2Ca^{2+}$/$2Sr^{2+}$ adsorbed onto (5,5) armchair SWCNT in aqueous medium by CAM-B3LYP functional and 6-31+G (2d,p), EPR-III, LANL2DZ basis sets.

Inhibitor → Al-Alloy	HOMO	LUMO	ΔE	μ	χ	H	ζ	ψ
Alendronate → $2Mg^{2+}$	−0.1160	0.2485	9.9188	1.8027	−1.8027	4.9594	0.1008	0.3276
Alendronate → $2Ca^{2+}$	−0.1006	0.0707	4.6594	−0.4068	0.4068	2.3297	0.2146	0.0355
Alendronate → $2Sr^{2+}$	−0.1086	0.2270	9.1340	1.6109	−1.6109	4.5670	0.1095	0.2841
Ibandronate → $2Mg^{2+}$	−0.1501	0.1772	8.9062	0.3687	−0.3687	4.4531	0.1123	0.0152
Ibandronate → $2Ca^{2+}$	−0.1265	0.0585	5.0352	−0.9252	0.9252	2.5176	0.1986	0.1700
Ibandronate → $2Sr^{2+}$	−0.0793	0.1429	6.0480	0.8653	−0.8653	3.0240	0.1653	0.1238
Neridronate → $2Mg^{2+}$	−0.1468	0.1609	8.3726	0.1918	−0.1918	4.1863	0.1194	0.0044
Neridronate → $2Ca^{2+}$	−0.1364	0.0450	4.9377	−1.2435	1.2435	2.4689	0.2025	0.3131
Neridronate → $2Sr^{2+}$	−0.0328	0.1890	6.0357	2.1252	−2.1252	3.0178	0.1657	0.7483
Pamidronate → $2Mg^{2+}$	−0.1052	0.1807	7.7824	1.0272	−1.0272	3.8912	0.1285	0.1356
Pamidronate → $2Ca^{2+}$	−0.1042	0.0834	5.1081	−0.2830	0.2830	2.5540	0.1957	0.0156
Pamidronate → $2Sr^{2+}$	−0.0581	0.1458	5.5489	1.1932	−1.1932	2.7744	0.1802	0.2566

$\Delta E = E_{LUMO} - E_{HOMO}$; $\mu = (E_{HOMO} + E_{LUMO})/2$; $\chi = -(E_{HOMO} + E_{LUMO})/2$; $\eta = (E_{LUMO} - E_{HOMO})/2$; $\zeta = 1/(2\eta)$; $\psi = \mu^2/(2\eta)$

LUMO, HOMO, and band energy gap (ev) indicated the pictorial explanation of the frontier molecular orbitals, which are an important factor for identifying the molecular characteristics of the drug delivery method though adsorbing the BP agents of alendronate, ibandronate, neridronate, and pamidronate chelated to $2Mg^{2+}$, $2Ca^{2+}$, and $2Sr^{2+}$, which have been surrounded by H_2O molecules on the (5,5) armchair SWCNT in aqueous medium (Figure 6).

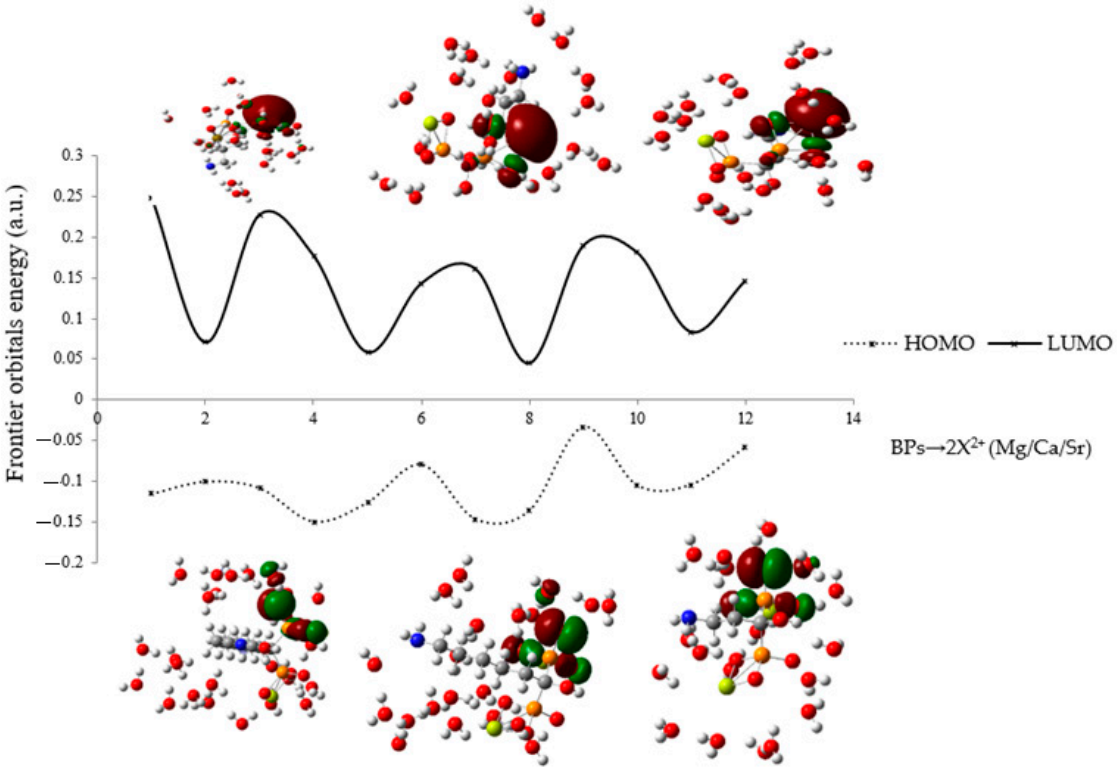

Figure 6. The energy gap of HOMO/LUMO (a.u.) for adsorbing alendronate, ibandronate, neridronate, and pamidronate chelated to $2Mg^{2+}$, $2Ca^{2+}$, and $2Sr^{2+}$ onto (5,5) armchair SWCNT in aqueous medium.

In this research, the energy gap appoints how BP agents of alendronate, ibandronate, neridronate, and pamidronate chelated to $2Mg^{2+}$, $2Ca^{2+}$, and $2Sr^{2+}$ can interact with (5,5) armchair SWCNT in aqueous medium. In addition, to attain more decisive approval in recognizing the specification of complexes of this structure, a group of chemical reactivity factors consisting of chemical potential (μ), electronegativity (χ), hardness (η), softness (ζ), and electrophilicity index (ψ) have been included (Table 4) [95–97]. The amounts of the parameters in Table 4 have exhibited good stability of BP agents through Langmuir adsorption on the (5,5) armchair SWCNT.

Molecular interactions are often related to the interaction energies, which, in turn, decide the Gibbs free energy of the incorporation of CNTs in the intercellular cavities. Moreover, hydrogen bonds play a vital role in the solubility of CNTs. Functionalization and composite formation with polymers increase the hydrogen bonding sites. Hydrogels help to increase the hydrophilicity of CNTs. As the number of hydrogen bonds increases, the solubility increases, which is essential for the interaction of CNTs with (alendronate/ibandronate/neridronate/pamidronate) → $2Mg^{2+}$/$2Ca^{2+}$/$2Sr^{2+}$ drugs. Although SWCNT might have higher interaction energy from van der Waals forces with chelated BPs with two metal cations $2Mg^{2+}$, $2Ca^{2+}$, and $2Sr^{2+}$ that can make them highly stable, the low electric potential extracts from electrostatic properties of NQR (Table 2 and Figure 3) for elements of BPs → $2Mg^{2+}$/$2Ca^{2+}$/$2Sr^{2+}$ in the aqueous medium, which have been adsorbed on the SWCNT surface, can indicate that van der Waals (vdW) energies might be neglected.

4. Conclusions

According to this research, by the incorporation of chelated $2Mg^{2+}$, $2Ca^{2+}$, and $2Sr^{2+}$ cations to BP drugs adsorbed onto (5,5) armchair SWCNT, the lattice compression would increase, owing to the larger atomic radius of Sr^{2+} cation rather than Ca^{2+} and Mg^{2+}, respectively.

The perspective of NMR spectroscopy has suggested the location of active sites of targeted N, P, O, and two metal cations of $2Mg^{2+}$, $2Ca^{2+}$, and $2Sr^{2+}$ in chelated alendronate, ibandronate, neridronate, and pamidronate complexes adsorbed onto (5,5) armchair SWCNT replaces the charge density in polar BPs in the aqueous medium toward (5,5) armchair CNT. For improving bone treatments, various investigations have concentrated on the substitution of $2Ca^{2+}$ cation by $2Sr^{2+}$ cation in the compound of bioactive glasses, which can be used for curing vertebral complex fractures.

Compared to ΔG_R^o amounts from infrared spectroscopy, an appropriate accord among computed consequences has been approved, as well as the accuracy of the chosen isotherm for (alendronate/ibandronate/neridronate/pamidronate) → $2Mg^{2+}$/$2Ca^{2+}$/$2Sr^{2+}$ adsorbed onto (5,5) armchair SWCNT in aqueous medium, with the most fluctuation in Gibbs free energy for BPs → $2Sr^{2+}$ at 300 K. In fact, the achieved results represented the feasibility of using (5,5) armchair SWCNT, and these compounds became the norm in the drug delivery system, which was attained by quantum calculations due to the physico-chemical properties of NMR and IR spectroscopies [98]. Finally, this work has approved that SWCNT can penetrate bone cells for the release of chelated BP–cations directly to bone tissue, which is based on a drug delivery method towards improving the pharmacological and therapeutic system.

Author Contributions: F.M.: Conceptualization and idea, Methodology, Software, Validation, Formal analysis, Investigation, Data curation, Writing—original draft preparation, Visualization, Supervision, Project administration. M.M.: Methodology, Software, Formal analysis, Investigation, Data curation, Writing—review and editing, Visualization, Resources. All authors have read and agreed to the published version of the manuscript.

Funding: This research received no external funding.

Data Availability Statement: Not applicable.

Acknowledgments: In successfully completing this paper and its research, the authors are grateful to Kastamonu University for support through the office, library, and scientific websites.

Conflicts of Interest: The authors declare no conflict of interest.

References

1. Kistler-Fischbacher, M.; Weeks, B.K.; Beck, B.R. The effect of exercise intensity on bone in postmenopausal women (part 2): A meta-analysis. *Bone* **2021**, *143*, 115697. [CrossRef] [PubMed]
2. Sun, K.; Liu, J.M.; Sun, H.X.; Lu, N.; Ning, G. Bisphosphonate treatment and risk of esophageal cancer: A meta-analysis of observational studies. *Osteoporos. Int.* **2013**, *24*, 279–286. [CrossRef]
3. Åkesson, K.E.; McGuigan, F.E.A. Closing the Osteoporosis Care Gap. *Curr. Osteoporos. Rep.* **2021**, *19*, 58–65. [CrossRef] [PubMed]
4. Mollaamin, F. On the Behavior of Boron Nitride Nanotube-Flavin Adenine Dinucleotide Interaction Ion Implantation Order to Design Biofuel Cells. *J. Comput. Theor. Nanosci.* **2014**, *11*, 2017–2022. [CrossRef]
5. Mollaamin, F. Chemotherapy Study of alkaloids through Theoretical Quantum Methods. *Moroc. J. Chem.* **2020**, *8*, 400–411. [CrossRef]
6. Li, J.; Zeng, M.; Shan, H.; Tong, C. Microneedle Patches as Drug and Vaccine Delivery Platform. *Curr. Med. Chem.* **2017**, *2*, 2413–2422. [CrossRef]
7. Mollaamin, F. Physicochemical investigation of anti-covid19 drugs using several medicinal plants. *J. Chil. Chem. Soc.* **2022**, *67*, 5537–5546. [CrossRef]
8. Mollaamin, F.; Shahriari, S.; Monajjemi, M. Treating omicron ba.4 & ba.5 via herbal antioxidant asafoetida: A dft study of carbon nanocarrier in drug delivery. *J. Chil. Chem. Soc.* **2023**, *68*, 5781–5786. [CrossRef]
9. Mollaamin, F.; Monajjemi, M. Thermodynamic research on the inhibitors of coronavirus through drug delivery method. *J. Chil. Chem. Soc.* **2021**, *66*, 5195–5205. [CrossRef]
10. Mollaamin, F.; Monajjemi, M. Graphene-based resistant sensor decorated with Mn, Co, Cu for nitric oxide detection: Langmuir adsorption & DFT method. *Sens. Rev.* 2023, *ahead-of-print*. [CrossRef]
11. Tahan, A.; Mollaamin, F.; Monajjemi, M. Thermochemistry and NBO analysis of peptide bond: Investigation of basis sets and binding energy. *Russ. J. Phys. Chem. A* **2009**, *83*, 587–597. [CrossRef]
12. Bakhshi, K.; Mollaamin, F.; Monajjemi, M. Exchange and Correlation Effect of Hydrogen Chemisorption on Nano V(100) Surface: A DFT Study by Generalized Gradient Approximation (GGA). *J. Comput. Theor. Nanosci.* **2011**, *8*, 763–768. [CrossRef]
13. Monajjemi, M.; Baie, M.T.; Mollaamin, F. Interaction between threonine and cadmium cation in [Cd(Thr)] (n = 1–3) complexes: Density functional calculations. *Russ. Chem. Bull.* **2010**, *59*, 886–889. [CrossRef]
14. Khalili Hadad, B.; Mollaamin, F.; Monajjemi, M. Biophysical chemistry of macrocycles for drug delivery: A theoretical study. *Russ. Chem. Bull.* **2011**, *60*, 238–241. [CrossRef]
15. Mohsin, S.M.N.; Hussein, M.Z.; Sarijo, S.H.; Fakurazi, S.; Arulselvan, P.; Taufiq-Yap, Y.H. Characterisation and Cytotoxicity Assessment of UV Absorbers-Intercalated Zinc/Aluminium-Layered Double Hydroxides on Dermal Fibroblast Cells. *Sci. Adv. Mater.* **2014**, *6*, 648–658. [CrossRef]
16. Monajjemi, M.; Mahdavian, L.; Mollaamin, F.; Khaleghian, M. Interaction of Na, Mg, Al, Si with carbon nanotube (CNT): NMR and IR study. *Russ. J. Inorg. Chem* **2009**, *54*, 1465–1473. [CrossRef]
17. Barahuie, F.; Hussein, M.Z.; Hussein-Al-Ali, S.H.; Arulselvan, P.; Fakurazi, S.; Zainal, Z. Preparation and controlled-release studies of a protocatechuic acid-magnesium/aluminumlayered double hydroxide nanocomposites. *Int. J. Nanomed.* **2013**, *8*, 1975–1987. [CrossRef]
18. Kura, A.U.; Ali, S.H.H.A.; Hussein, M.Z.; Fakurazi, S.; Arulselvan, P. Development of a controlled-release anti-parkinsonian nanodelivery system using levodopa as the active agent. *Int. J. Nanomed.* **2013**, *8*, 1103–1110. [CrossRef]
19. Mohsin, S.M.N.; Hussein, M.Z.; Sarijo, S.H.; Fakurazi, S.; Arulselvan, P.; Hin, T.-Y. Synthesis of (cinnamate-zinc layered hydroxide) intercalation compound for sunscreen application. *Chem. Cent. J.* **2013**, *7*, 26. [CrossRef]
20. Mohsin, S.M.N.; Hussein, M.Z.; Sarijo, S.H.; Fakurazi, S.; Arulselvan, P.; Taufiq-Yap, Y.H. Optimization of UV absorptivity of layered double hydroxide by intercalating organic UV-absorbent molecules. *J. Biomed. Nanotechnol.* **2014**, *10*, 1490–1500. [CrossRef]
21. Cao, X.; Deng, W.; Fu, M.; Zhu, Y.; Liu, H.; Wang, L.; Zeng, J.; Wei, Y.; Xu, X.; Yu, J. Seventy-two-hour release formulation of the poorly soluble drug silybin based on porous silica nanoparticles: In vitro release kinetics and in vitro/in vivo correlations in beagle dogs. *Eur. J. Pharm. Sci.* **2013**, *48*, 64–71. [CrossRef] [PubMed]
22. Ghaffarian, R.; Bhowmick, T.; Muro, S. Transport of nanocarriers across gastrointestinal epithelial cells by a new transcellular route induced by targeting ICAM-1. *J. Control. Release* **2012**, *163*, 25–33. [CrossRef] [PubMed]
23. Zhang, L.; Xue, H.; Cao, Z.; Keefe, A.; Wang, J.; Jiang, S. Multifunctional and degradable zwitterionic nanogels for targeted delivery, enhanced MR imaging, reduction-sensitive drug release, and renal clearance. *Biomaterials* **2011**, *32*, 4604–4608. [CrossRef] [PubMed]
24. Bethune, D.S.; Kiang, C.H.; de Vries, M.S.; Gorman, G.; Savoy, R.; Vazquez, J.; Beyers, R. Cobalt-catalysed growth of carbon nanotubes with single-atomic-layer walls. *Nature* **1993**, *363*, 605–607. [CrossRef]
25. Iijima, S.; Ichihashi, T. Single-shell carbon nanotubes of 1-nm diameter. *Nature* **1993**, *363*, 603–605. [CrossRef]

26. Dai, H. Carbon nanotubes: Opportunities and challenges. *Surf. Sci.* **2002**, *500*, 218–241. [CrossRef]
27. Abi, T.G.; Karmakar, T.; Taraphder, S. Proton affinity of polar amino acid sidechain analogues anchored to the outer wall of single walled carbon nanotubes. *Comput. Theor. Chem.* **2013**, *1010*, 53–66. [CrossRef]
28. Feng, W.; Ji, P. Enzymes immobilized on carbon nanotubes. *Biotechnol. Adv.* **2011**, *29*, 889–895. [CrossRef]
29. Chen, Q.; Kaneko, T.; Hatakeyama, R. Characterization of pulse-driven gas-liquid interfacial discharge plasmas and application to synthesis of gold nanoparticle-DNA encapsulated carbon nanotubes. *Curr. Appl. Phys.* **2011**, *11*, S63–S66. [CrossRef]
30. Ghalandari, B.; Monajjemi, M.; Mollaamin, F. Theoretical Investigation of Carbon Nanotube Binding to DNA in View of Drug Delivery. *J. Comput. Theor. Nanosci.* **2011**, *8*, 1212–1219. [CrossRef]
31. Khaleghian, M.; Zahmatkesh, M.; Mollaamin, F.; Monajjemi, M. Investigation of Solvent Effects on Armchair Single-Walled Carbon Nanotubes: A QM/MD Study. *Full-Nanotub. Carbon Nanostruct.* **2011**, *19*, 251–261. [CrossRef]
32. Monajjemi, M.; Khaleghian, M.; Tadayonpour, N.; Mollaamin, F. The effect of different solvents and temperatures on stability of single-walled carbon nanotube: A QM/MD study. *Int. J. Nanosci.* **2010**, *9*, 517–529. [CrossRef]
33. Mollaamin, F.; Monajjemi, M.; Salemi, S.; Baei, M.T. A Dielectric Effect on Normal Mode Analysis and Symmetry of BNNT Nanotube. *Full-Nanotub. Carbon Nanostruct.* **2011**, *19*, 182–196. [CrossRef]
34. Mollaamin, F.; Monajjemi, M. In Silico-DFT Investigation of Nanocluster Alloys of Al-(Mg, Ge, Sn) Coated by Nitrogen Heterocyclic Carbenes as Corrosion Inhibitors. *J. Clust. Sci.* **2023**. [CrossRef]
35. Sapino, S.; Chindamo, G.; Chirio, D.; Manzoli, M.; Peira, E.; Riganti, C.; Gallarate, M. Calcium Phosphate-Coated Lipid Nanoparticles as a Potential Tool in Bone Diseases Therapy. *Nanomaterials* **2021**, *11*, 2983. [CrossRef]
36. Park, J.; Cimpean, A.; Tesler, A.B.; Mazare, A. Anodic TiO_2 Nanotubes: Tailoring Osteoinduction via Drug Delivery. *Nanomaterials* **2021**, *11*, 2359. [CrossRef]
37. Gao, L.; Zhang, S.-Q. Antiosteoporosis Effects, Pharmacokinetics, and Drug Delivery Systems of Icaritin: Advances and Prospects. *Pharmaceuticals* **2022**, *15*, 397. [CrossRef]
38. Chindamo, G.; Sapino, S.; Peira, E.; Chirio, D.; Gonzalez, M.C.; Gallarate, M. Bone Diseases: Current Approach and Future Perspectives in Drug Delivery Systems for Bone Targeted Therapeutics. *Nanomaterials* **2020**, *10*, 875. [CrossRef]
39. Salamanna, F.; Gambardella, A.; Contartese, D.; Visani, A.; Fini, M. Nano-Based Biomaterials as Drug Delivery Systems Against Osteoporosis: A Systematic Review of Preclinical and Clinical Evidence. *Nanomaterials* **2021**, *11*, 530. [CrossRef]
40. Choi, S.; Jo, H.-S.; Song, H.; Kim, H.-J.; Oh, J.-K.; Cho, J.-W.; Park, K.; Kim, S.-E. Multifunctional Tannic Acid-Alendronate Nanocomplexes with Antioxidant, Anti-Inflammatory, and Osteogenic Potency. *Nanomaterials* **2021**, *11*, 1812. [CrossRef]
41. Monajjemi, M. Cell membrane causes the lipid bilayers to behave as variable capacitors: A resonance with self-induction of helical proteins. *Biophys. Chem.* **2015**, *207*, 114–127. [CrossRef] [PubMed]
42. Mahdavian, L.; Monajjemi, M. Alcohol sensors based on SWNT as chemical sensors: Monte Carlo and Langevin dynamics simulation. *Microelectron. J.* **2010**, *41*, 142–149. [CrossRef]
43. Monajjemi, M.; Farahani, N.; Mollaamin, F. Thermodynamic study of solvent effects on nanostructures: Phosphatidylserine and phosphatidylinositol membranes. *Phys. Chem. Liq.* **2012**, *50*, 161–172. [CrossRef]
44. Sarasia, E.M.; Afsharnezhad, S.; Honarparvar, B.; Mollaamin, F.; Monajjemi, M. Theoretical study of solvent effect on NMR shielding tensors of luciferin derivatives. *Phys. Chem. Liq.* **2011**, *49*, 561–571. [CrossRef]
45. Mollaamin, F.; Monajjemi, M. Application of DFT/TD-DFT Frameworks in the Drug Delivery Mechanism: Investigation of Chelated Bisphosphonate with Transition Metal Cations in Bone Treatment. *Chemistry* **2023**, *5*, 365–380. [CrossRef]
46. Mollaamin, F.; Ilkhani, A.R.; Sakhaei, N.; Bonsakhteh, B.; Faridchehr, A.; Tohidi, S.; Monajjemi, M. Thermodynamic and Solvent Effect on Dynamic Structures of Nano Bilayer-Cell Membrane: Hydrogen Bonding Study. *J. Comput. Theor. Nanosci.* **2015**, *12*, 3148–3154. [CrossRef]
47. Mbese, Z.; Aderibigbe, B.A. Bisphosphonate-Based Conjugates and Derivatives as Potential Therapeutic Agents in Osteoporosis, Bone Cancer and Metastatic Bone Cancer. *Int. J. Mol. Sci.* **2021**, *22*, 6869. [CrossRef]
48. Rauner, M.; Taipaleenmäki, H.; Tsourdi, E.; Winter, E.M. Osteoporosis Treatment with Anti-Sclerostin Antibodies—Mechanisms of Action and Clinical Application. *J. Clin. Med.* **2021**, *10*, 787. [CrossRef]
49. Geiger, I.; FLS-CARE study group; Kammerlander, C.; Höfer, C.; Volland, R.; Trinemeier, J.; Henschelchen, M.; Friess, T.; Böcker, W.; Sundmacher, L. Implementation of an integrated care programme to avoid fragility fractures of the hip in older adults in 18 Bavarian hospitals–study protocol for the cluster-randomised controlled fracture liaison service FLS-CARE. *BMC Geriatr.* **2021**, *21*, 43. [CrossRef]
50. Hayes, K.N.; He, N.; Brown, K.A.; Cheung, A.M.; Juurlink, D.N.; Cadarette, S.M. Over half of seniors who start oral bisphosphonate therapy are exposed for 3 or more years: Novel rolling window approach and patterns of use. *Osteoporos. Int.* **2021**, *32*, 1413–1420. [CrossRef]
51. Sølling, A.S.; Christensen, D.H.; Darvalics, B.; Harsløf, T.; Thomsen, R.W.; Langdahl, B. Fracture rates in patients discontinuing alendronate treatment in real life: A population-based cohort study. *Osteoporos. Int.* **2021**, *32*, 1103–1115. [CrossRef]
52. Kim, J.-W.; Yee, J.; Oh, S.-H.; Kim, S.-H.; Kim, S.-J.; Chung, J.-E.; Gwak, H.-S. Machine Learning Approaches for Predicting Bisphosphonate-Related Osteonecrosis in Women with Osteoporosis Using *VEGFA* Gene Polymorphisms. *J. Pers. Med.* **2021**, *11*, 541. [CrossRef]
53. Langdahl, B.L. Overview of treatment approaches to osteoporosis. *Br. J. Pharmacol.* **2021**, *178*, 1891–1906. [CrossRef]

54. Widler, L.; Jaeggi, K.A.; Glatt, M.; Müller, K.; Bachmann, R.; Bisping, M.; Born, A.-R.; Cortesi, R.; Guiglia, G.; Jeker, H.; et al. Highly Potent Geminal Bisphosphonates. From Pamidronate Disodium (Aredia) to Zoledronic Acid (Zometa). *J. Med. Chem.* **2002**, *45*, 3721–3738. [CrossRef]
55. Thompson, K.; Rogers, M.J. The Molecular Mechanisms of Action of Bisphosphonates. *Clin. Rev. Bone Miner. Metab.* **2007**, *5*, 130–144. [CrossRef]
56. Russell, R.G.; Watts, N.B.; Ebetino, F.H.; Rogers, M.J. Mechanisms of action of bisphosphonates: Similarities and differences and their potential influence on clinical efficacy. *Osteoporos. Int.* **2008**, *19*, 733–759. [CrossRef]
57. Russell, R.G. Bisphosphonates: The first 40 years. *Bone* **2011**, *49*, 2–19. [CrossRef]
58. Quesnel, A.M.; Seton, M.; Merchant, S.N.; Halpin, C.; McKenna, M.J. Third generation bisphosphonates for treatment of sensorineural hearing loss in otosclerosis. *Otol. Neurotol.* **2012**, *33*, 1308–1314. [CrossRef]
59. Diez-Perez, A. Bisphosphonates. *Maturitas* **2002**, *43*, S19. [CrossRef]
60. Rodríguez-Lorenzo, L.M.; Vazquez, B.; San Román, J.; Gross, K.A. Incorporation of 2nd and 3rd Generation Bisphosphonates on Hydroxyfluorapatite. *Key Eng. Mater.* **2006**, *309–311*, 899–902.
61. Mollaamin, F.; Özcan, S.; Özcan, E.; Monajjemi, M. Biomedical Applications of Bisphosphonate Chelating Agents by Metal Cations as Drug Design for Prevention and Treatment of Osteoporosis using QM/MM Method. *Biointerface Res. Appl. Chem.* **2023**, *13*, 329. [CrossRef]
62. Lenart, B.A.; Lorich, D.G.; Lane, J.M. Atypical Fractures of the Femoral Diaphysis in Postmenopausal Women Taking Alendronate. *N. Engl. J. Med.* **2008**, *358*, 1304–1306. [CrossRef] [PubMed]
63. Kwek, E.B.; Goh, S.K.; Koh, J.S.; Png, M.A.; Howe, T.S. An emerging pattern of subtrochanteric stress fractures: A long-term complication of alendronate therapy? *Injury* **2008**, *39*, 224–231. [CrossRef] [PubMed]
64. Bauss, F.; Schimmer, R.C. Ibandronate: The first once-monthly oral bisphosphonate for treatment of postmenopausal osteoporosis. *Ther. Clin. Risk Manag.* **2006**, *2*, 3–18.
65. Sittig, H.-B. Pathogenesis and Bisphosphonate Treatment of Skeletal Events and Bone Pain in Metastatic Cancer: Focus on Ibandronate. *Onkologie* **2012**, *35*, 380–387. [CrossRef]
66. Gatti, D.; Viapiana, O.; Idolazzi, L.; Fracassi, E.; Adami, S. Neridronic acid for the treatment of bone metabolic diseases. *Expert Opin. Drug Metab. Toxicol.* **2009**, *5*, 1305–1311. [CrossRef]
67. Varenna, M.; Adami, S.; Rossini, M.; Gatti, D.; Idolazzi, L.; Zucchi, F.; Malavolta, N.; Sinigaglia, L. Treatment of complex regional pain syndrome type I with neridronate: A randomized, double-blind, placebo-controlled study. *Rheumatology* **2013**, *52*, 534–542. [CrossRef]
68. Kubalek, I.; Fain, O.; Paries, J.; Kettaneh, A.; Thomas, M. Treatment of reflex sympathetic dystrophy with pamidronate: 29 cases. *Rheumatology* **2001**, *40*, 1394–1397. [CrossRef]
69. Zarychanski, R.; Elphee, E.; Walton, P.; Johnston, J. Osteonecrosis of the jaw associated with pamidronate therapy. *Am. J. Hematol.* **2006**, *81*, 73–75. [CrossRef]
70. Frisch, M.J.; Trucks, G.W.; Schlegel, H.B.; Scuseria, G.E.; Robb, M.A.; Cheeseman, J.R.; Scalmani, G.; Barone, V.; Petersson, G.A.; Nakatsuji, H.; et al. *Gaussian 16, Revision C.01*; Gaussian, Inc.: Wallingford, CT, USA, 2016.
71. Becke, A.D. Density-functional thermochemistry. III. The role of exact exchange. *J. Chem. Phys.* **1993**, *98*, 5648–5652. [CrossRef]
72. Lee, C.; Yang, W.; Parr, R.G. Development of the Colle-Salvetti correlation-energy formula into a functional of the electron density. *Phys. Rev. B* **1988**, *37*, 785–789. [CrossRef]
73. Koch, W.; Holthausen, M.C. *A Chemist's Guide to Density Functional Theory*, 2nd ed.; Wiley-VCH: Weinheim, Germany, 2000; pp. 3–64, 93–104.
74. Monajjemi, M.; Mollaamin, F.; Shojaei, S. An overview on coronaviruses family from past to COVID-19: Introduce some inhibitors as antiviruses from Gillan's plants. *Biointerface Res. Appl. Chem.* **2020**, *3*, 5575–5585. [CrossRef]
75. Zadeh, M.A.A.; Lari, H.; Kharghanian, L.; Balali, E.; Khadivi, R.; Yahyaei, H.; Mollaamin, F.; Monajjemi, M. Density Functional Theory Study and Anti-Cancer Properties of Shyshaq Plant: In View Point of Nano Biotechnology. *J. Comput. Theor. Nanosci.* **2015**, *12*, 4358–4367. [CrossRef]
76. Monajjemi, M.; Shahriari, S.; Mollaamin, F. Evaluation of Coronavirus Families & Covid-19 Proteins: Molecular Modeling Study. *Biointerface Res. Appl. Chem.* **2020**, *10*, 6039–6057. [CrossRef]
77. Monajjemi, M.; Noei, M. Mollaamin, F. Design of fMet-tRNA and Calculation of its Bonding Properties by Quantum Mechanics. *Nucleosides Nucleotides Nucleic Acids* **2010**, *29*, 676–683. [CrossRef]
78. Cramer, C.J.; Truhlar, D.G. PM3-SM3: A general parameterization for including aqueous solvation effects in the PM3 molecular orbital model. *J. Comp. Chem.* **1992**, *13*, 1089. [CrossRef]
79. Liotard, D.A.; Hawkins, G.D.; Lynch, G.C.; Cramer, C.J.; Truhlar, D.G. Improved methods for semiempirical solvation models. *J. Comp. Chem.* **1995**, *16*, 422. [CrossRef]
80. Chambers, C.C.; Hawkins, G.D.; Cramer, C.J.; Truhlar, D.G. Model for aqueous solvation based on class IV atomic charges and first solvation shell effects. *J. Phys. Chem.* **1996**, *100*, 16385. [CrossRef]
81. Giesen, D.J.; Gu, M.Z.; Cramer, C.J.; Truhlar, D.G. A universal organic solvation model. *J. Org. Chem.* **1996**, *61*, 8720. [CrossRef]
82. Mollaamin, F.; Monajjemi, M. Tailoring and functionalizing the graphitic-like GaN and GaP nanostructures as selective sensors for NO, NO2, and NH3 adsorbing: A DFT study. *J. Mol. Model.* **2023**, *29*, 170. [CrossRef]

83. Mollaamin, F.; Monajjemi, M. Transition metal (X = Mn, Fe, Co, Ni, Cu, Zn)-doped graphene as gas sensor for CO2 and NO2 detection: A molecular modeling framework by DFT perspective. *J. Mol. Model.* **2023**, *29*, 119. [CrossRef] [PubMed]
84. Tanaka, S.; Tanaka, Y. RANKL as a therapeutic target of rheumatoid arthritis. *J. Bone Miner. Metab.* **2021**, *39*, 106–112. [CrossRef] [PubMed]
85. Mollaamin, F.; Monajjemi, M. Harmonic Linear Combination and Normal Mode Analysis of Semiconductor Nanotubes Vibrations. *J. Comput. Theor. Nanosci.* **2015**, *12*, 1030–1039. [CrossRef]
86. Rauch, L.; Hein, R.; Biedermann, T.; Eyerich, K.; Lauffer, F. Bisphosphonates for the Treatment of Calcinosis Cutis—A Retrospective Single-Center Study. *Biomedicines* **2021**, *9*, 1698. [CrossRef] [PubMed]
87. Monajjemi, M. Metal-doped graphene layers composed with boron nitride–graphene as an insulator: A nano-capacitor. *J. Mol. Model.* **2014**, *20*, 1–8. [CrossRef] [PubMed]
88. Fry, A.R.; Kwon, K.D.; Komarneni, S.; Kubicki, J.D.; Mueller, K.T. Solid-State NMR and Computational Chemistry Study of Mononucleotides Adsorbed to Alumina. *Langmuir* **2006**, *22*, 9281–9286. [CrossRef]
89. Smith, J.A.S. Nuclear Quadrupole Resonance Spectroscopy. *J. Chem. Educ.* **1971**, *48*, 39–41. [CrossRef]
90. Mollaamin, F.; Shahriari, S.; Monajjemi, M.; Khalaj, Z. Nanocluster of Aluminum Lattice via Organic Inhibitors Coating: A Study of Freundlich Adsorption. *J. Clust. Sci.* **2023**, *34*, 1547–1562. [CrossRef]
91. Mollaamin, F.; Monajjemi, M. Molecular modelling framework of metal-organic clusters for conserving surfaces: Langmuir sorption through the TD-DFT/ONIOM approach. *Mol. Simul.* **2023**, *49*, 365–376. [CrossRef]
92. Young, H.A.; Freedman, R.D. *Sears and Zemansky's University Physics with Modern Physics*, 13th ed.; Addison-Wesley: Boston, MA, USA, 2012; p. 754.
93. Kołodziejska, B.; Stępień, N.; Kolmas, J. The Influence of Strontium on Bone Tissue Metabolism and Its Application in Osteoporosis Treatment. *Int. J. Mol. Sci.* **2021**, *22*, 6564. [CrossRef]
94. Marx, D.; Yazdi, A.R.; Papini, M.; Towler, M. A review of the latest insights into the mechanism of action of strontium in bone. *Bone Rep.* **2020**, *12*, 100273. [CrossRef]
95. Aihara, J.-I. Reduced HOMO−LUMO Gap as an Index of Kinetic Stability for Polycyclic Aromatic Hydrocarbons. *J. Phys. Chem. A* **1999**, *103*, 7487–7495. [CrossRef]
96. Parr, R.G.; Pearson, R.G. Absolute hardness: Companion parameter to absolute electronegativity. *J. Am. Chem. Soc.* **1983**, *105*, 7512–7516. [CrossRef]
97. Politzer, P.; Abu-Awwad, F. A comparative analysis of Hartree-Fock and Kohn-Sham orbital energies. *Theor. Chem. Accounts* **1998**, *99*, 83–87. [CrossRef]
98. Mollaamin, F. Features of Parametric Point Nuclear Magnetic Resonance of Metals Implantation on Boron Nitride Nanotube by Density Functional Theory/Electron Paramagnetic Resonance. *J. Comput. Theor. Nanosci.* **2014**, *11*, 2393–2398. [CrossRef]